

# Grain size dependent strain rate sensitivity in nanocrystalline body-centered cubic metal thin films

Q. Zhou<sup>a</sup>, J. Zhao<sup>b</sup>, J.Y. Xie<sup>a</sup>, F. Wang<sup>b,\*</sup>, P. Huang<sup>a,\*</sup>, T.J. Lu<sup>b</sup>, K.W. Xu<sup>a</sup>

<sup>a</sup> State-Key Laboratory for Mechanical Behavior of Material, Xi'an Jiaotong University, Xi'an 710049, China

<sup>b</sup> State-Key Laboratory for Strength and Vibration of Mechanical Structures, School of Aerospace, Xi'an Jiaotong University, Xi'an 710049, China

## ARTICLE INFO

### Article history:

Received 27 February 2014

Accepted 21 April 2014

Available online 30 April 2014

### Keywords:

Strain rate sensitivity

Nanocrystalline

Nanoindentation

Grain size dependence

## ABSTRACT

The strain rate sensitivity ( $m$ ) and activation volume ( $v^*$ ) of three nanocrystalline (NC) body-centered cubic (bcc) metals, i.e., W, Mo and Ta, with various grain sizes were evaluated by nanoindentation testing. Opposite to the conventional trend that NC bcc metals exhibit reduced  $m$  as the grain size was decreased, elevated  $m$  was observed as the grain size was reduced from  $\sim 90$  nm to  $\sim 30$  nm for all the samples concerned. It was proposed that the unusual variation trends of  $m$  for NC bcc metals were dominated by GB-related mechanisms when the grain size drops below a critical value.

© 2014 Elsevier B.V. All rights reserved.

## 1. Introduction

Because of the confined nanoscale intragranular structure and enhanced grain boundary (GB) activities, the mechanical properties of nanocrystalline (NC) metals have been extensively studied in recent years [1–3]. For NC metals, GB-mediated mechanisms such as GB sliding, Coble creep and GB rotation played a key role during plastic deformation. The strain rate sensitivity  $m$  and apparent activation volume  $v^*$  of a NC metal were two crucial parameters that could shed light on its rate controlling deformation mechanisms during plastic deformation. Decreasing grain size led to increasing volume fraction of GBs, which would change dramatically  $m$  and apparent  $v^*$  relative to their bulk counterparts. Whilst existing studies concerning the variation trends of  $m$  and  $v^*$  focused mainly on face-centered cubic (fcc) metals, few concerned NC metals having body-centered cubic (bcc) lattice structures.

For NC fcc metals, e.g., Cu [4–6], Al [7,8] and Ni [9,10],  $m$  increased with decreasing grain size as shown in Fig. 1a. The enhancement was attributed to highly localized dislocation activities, such as dislocation nucleation from and/or dislocation de-pinning at GBs [9,11,12]. In contrast to fcc metals, as shown in Fig. 1b, bcc metals (e.g., Fe [13,14], Ta [4,15], W [16] and V [17]) exhibited a considerably reduced  $m$  as the grain size was reduced from coarse to ultra-fined or even nanoscale grains [4]. It was proposed that, as the grain size was reduced, the low mobility of screw dislocations played a crucial role for the reduced  $m$  [4]. However, a few exceptions opposing the

reducing trend of  $m$  in bcc metals were also reported: for instance, an unusual enhanced  $m$  was observed in ball-milled Fe powder particles when the grain size was reduced to nanoscale [18]. Apparently, the variation trend of  $m$  and related deformation mechanisms in bcc NC metals needed to be explored further.

In the present study, the strain rate sensitivity and apparent activation volume of NC W, Ta and Mo thin films were examined under nanoindentation testing. Special focus was placed upon the contribution of elevated volume fraction of GBs and confined nanoscale granular structure to the plastic deformation of the selected NC bcc metals.

## 2. Experimental

A series of W, Ta and Mo thin films (total thickness  $1 \mu\text{m}$ ) were deposited on Si (100) substrate by *d.c.* magnetron sputtering. The base pressure prior to sputtering was  $6.3 \times 10^{-5}$  Pa and Ar pressure during sputtering was  $5.4 \times 10^{-1}$  Pa. The deposition rates were 5 nm/min for W, 9 nm/min for Ta, and 7 nm/min for Mo films. In addition, another Mo film with much smaller grain size was deposited by hundreds short depositions separated by dwell intervals of 100 s as described in Ref. [19]. All the specimens were annealed at temperature ranging from 573 K to 1073 K for 30 min. The microstructures of the samples were investigated by means of X-ray diffraction (XRD), transmission electron microscopy (TEM, JEM200CX) and high resolution TEM (JEOL 2100F) operating at 200 kV. All the TEM foils were prepared via Gatan Precision Ion Polishing System 691 using Ar ion.

Indentation experiments were performed using a dynamic contact module device equipped with the Nanoindenter XP system

\* Corresponding authors.

E-mail addresses: [wangfei@mail.xjtu.edu.cn](mailto:wangfei@mail.xjtu.edu.cn) (F. Wang), [huangping@mail.xjtu.edu.cn](mailto:huangping@mail.xjtu.edu.cn) (P. Huang).

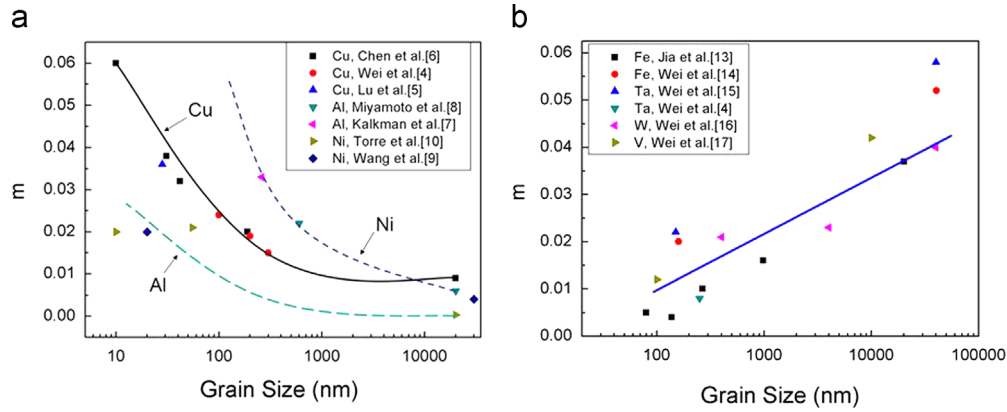


Fig. 1. Strain-rate sensitivity of (a) fcc metals and (b) bcc metals summarized using data from existing literatures.

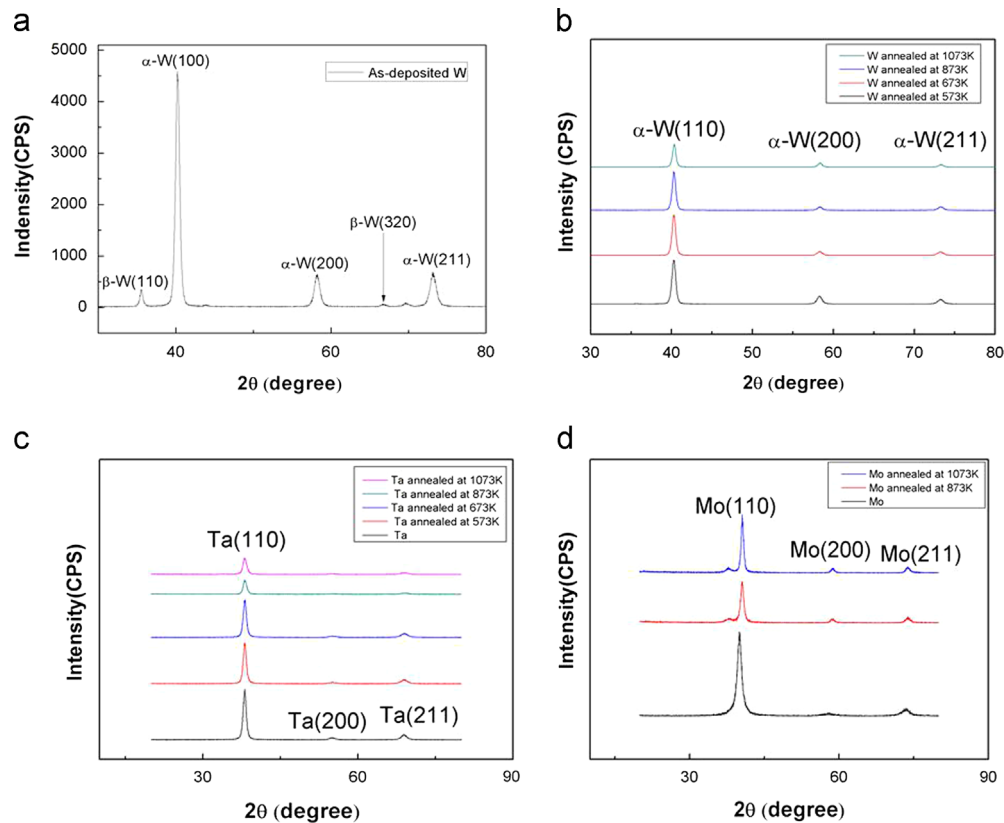


Fig. 2. X-ray diffraction scan for (a) as-deposited W films, (b) annealed W films, (c) Ta films and (d) Mo thin films.

(MTS, Inc.), under continuous stiffness measurement (CSM) mode at room temperature. Upon calibration on standard fused silicon, the tip of the Berkovich diamond indenter was estimated to have a radius of  $\sim 50$  nm. The hardness of the prepared thin films was examined using depth control mode at varying loading strain rate (LSR) from  $0.001$  to  $0.2 \text{ s}^{-1}$ , and the LSR  $\dot{\epsilon}$  was given by [20]:

$$\dot{\epsilon} = \frac{1}{h} \frac{\partial h}{\partial t} \quad (1)$$

where  $h$  was the indentation penetrating depth and  $t$  was time. The maximum penetration depth for all the indentation tests was set at  $200$  nm; and the hardness measured by CSM mode was calculated by averaging the hardness values obtained by varying the penetration depth from  $100$  to  $150$  nm to avoid the substrate effect. After the indenter reached the prescribed depth limit, the indenter was

unloaded to  $10\%$  of the maximum load and held for thermal drift correction before the indenter was withdrawn from the sample surface to terminate the indentation test. At each LSR for every sample, at least  $15$  effective indentation tests were conducted and used for subsequent analysis.

### 3. Results and discussion

XRD analysis shown in Fig. 2a indicated that whilst peaks of both  $\alpha$ -W (bcc structure) and  $\beta$ -W (A15 cubic lattice) existed in as-deposited W films, only  $\alpha$ -W appeared in annealed W films as shown in Fig. 2b. Therefore, in subsequent analysis, we only examined the annealed W films. In addition, the XRD patterns shown in Figs. 2c and d suggested that both Ta and Mo films had bcc structure.

The grain sizes ( $d$ ) of the prepared samples were estimated by TEM analysis. For W films annealed at 573 K and 1073 K, representative plan-view TEM bright-field micrographs and the

corresponding electron diffraction patterns were presented in Figs. 3a and b, respectively. Similarly, representative plan-view TEM bright-field micrographs of as-deposited Ta and

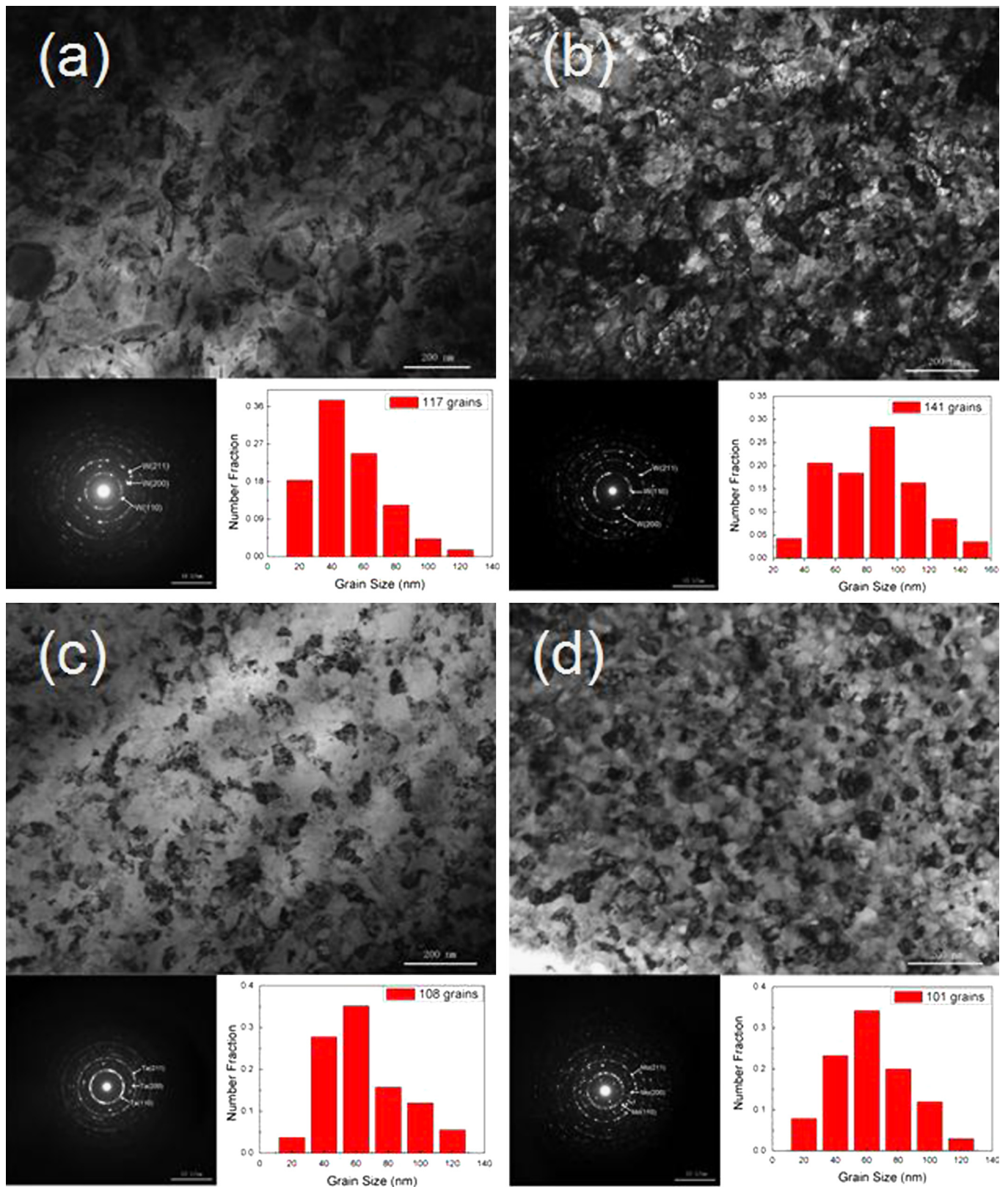


**Fig. 3.** TEM bright-field micrograph, electron diffraction pattern and grain size distribution of (a) 573 K annealed W, (b) 1073 K annealed W; (c) as-deposited Ta and (d) 1073 K annealed Mo thin films.

**Table 1**  
Grain sizes (average, estimated using TEM analysis) for W, Ta and Mo thin films.

Sample	Annealed temperature (K)	Grain size $d$ (nm) TEM
W	573	49.5
W	673	66
W	873	76.5
W	1073	88.1
Ta	As-deposited	55
Ta	573	44.4
Ta	673	47.3
Ta	873	43.8
Ta	1073	35.4
Mo	Deposition with short intervals	27.4
Mo	As-deposited	34.8
Mo	873	49.8
Mo	1073	63.9

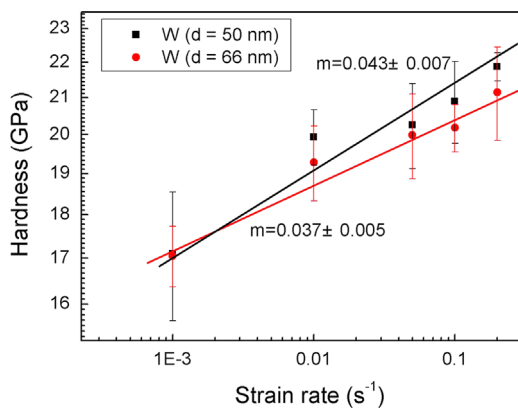


**Fig. 4.** Hardness plotted as a function of LSR for W thin films having different grain sizes.

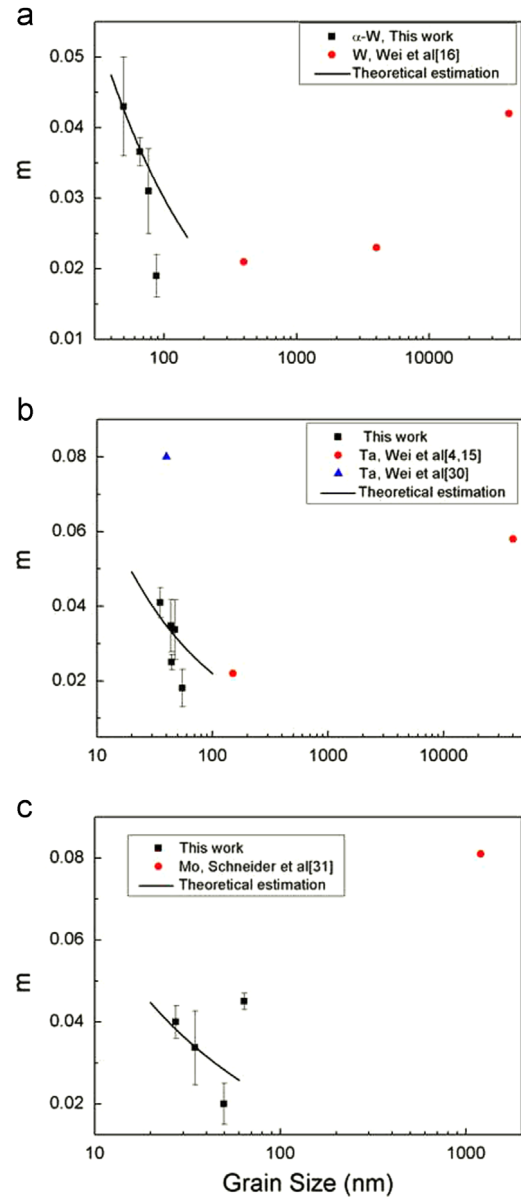
1073 K annealed Mo were shown in Figs. 3c and d, respectively. Upon systematically analyzing the plan-view grain sizes of all the samples prepared, the average grain sizes were listed in Table 1.

Fig. 4 plotted the measured hardness value of W thin films as a function of LSR on double-logarithmic scales. The hardness of 50 nm grained W changed from  $\sim 17.10$  GPa at LSR of  $10^{-3} \text{ s}^{-1}$  to  $\sim 21.87$  GPa at LSR of  $0.2 \text{ s}^{-1}$ , whilst the LSR dependence of the hardness of 66 nm grained W was less significant. Correspondingly, based on the equation:

$$m = \frac{\partial \ln H}{\partial \ln \dot{\epsilon}} \quad (2)$$

where  $H$  was the hardness and  $\dot{\epsilon}$  was the LSR, the rate sensitivity of the flow stress of W films having grain size of 50 nm and 66 nm was estimated to be  $0.043 \pm 0.007$  and  $0.037 \pm 0.005$ , respectively. In an identical way, the rate sensitivities of flow stress of NC Mo and Ta films were calculated from double logarithmic hardness vs. LSR curves. As the grain size of Mo films was reduced from 49.8 nm to 27.4 nm, the  $m$  value increased from  $0.022 \pm 0.005$  to  $0.041 \pm 0.004$  and the rate sensitivities were all significantly smaller than 0.085 obtained for coarse-grained Mo reported [21]. The variation trends of strain rate sensitivity with grain size for the three NC bcc samples were presented in Fig. 5.

As shown in Fig. 5, based on the values of  $m$  derived from the present study along with literature data, inflections appeared in all the NC bcc metals selected. The inflections of W, Ta and Mo appeared at about 90, 60 and 50 nm, which might be closely related to the critical grain size  $d_c$ , a specific parameter for bcc



**Fig. 5.** Strain rate sensitivity  $m$  plotted as a function of grain size  $d$  for (a) W, (b) Ta and (c) Mo thin films [30,31].

metals as discussed later in this paper. Meanwhile, the existence of the inflection indicated that the rate sensitivity of flow stress in bcc metals may not decrease monotonously with decreasing grain size.

The variation trend of  $m$  in ultra-fine grained and NC Fe (with bcc structure) as the grain size  $d$  was reduced from 80 nm to  $20 \mu\text{m}$  was reported by Jia et al. [13] and the samples prepared by ball milling were tested under uniaxial compression. It was found that  $m$  decreased continuously with decreasing  $d$ , dropping by one order of magnitude relative to  $\sim 0.04$  for conventional Fe. In addition, Wei et al. [4] investigated the response of ECAP Fe ( $d \sim 300$  nm) under compression and found its  $m$  value was obviously smaller than that of coarse-grained Fe. Nonetheless, an unusual enhanced  $m$  was detected when  $d$  was reduced to  $\sim 10$  nm in NC Fe. The unusual  $m$  value for Fe as  $d$  decreased into the NC regime was also detected by Malow and Koch [22].

For coarse-grained bcc metals, the Burgers vector of a bcc lattice lay along the [1 1 1] direction, which was the zone axis of three equivalent slip planes of the (1 1 0) family. In this way, the

core of screw dislocations in bcc metals was non-planar, spread in all the three (1 1 0) planes [23]. The peculiar non-planar dislocation core then led to a very large Peierls–Nabarro stress at low temperature, and the mobility of the screws was much smaller than that of edge dislocations [24]. Typically, the motion of screw dislocations in bcc metals was mediated by the double-kink mechanism. Since the nucleation of kink pairs could be assisted by thermal activation, the motion of screw dislocations also exhibited a strong dependence on rate sensitivity. According to Becker's theory, the apparent activation volume may be written as [25]:

$$v^* = b\xi l^* \quad (3)$$

where  $b$  is the Burgers vector of the dislocations,  $\xi$  representing the critical unzipping distance for a screw dislocation was the height of a kink (equaling to one atomic distance at a given temperature), and  $l^*$  is the critical distance between two kinks in a

kink pair. The activation volume was associated with plastic deformation and  $m$  was related via:

$$m = \frac{2.7\sqrt{3}K_b T}{Hv^*} \quad (4)$$

The critical thermally activated process in a bcc lattice structure was kink nucleation controlled, maintaining the rate-limiting step for a wide range of large grain sizes [26]. It was suggested [27,28] that the critical distance  $l^*$  between two kinks in a kink pair depended strongly on the applied stress  $\sigma$ , as follows:

$$l^* = \left( \frac{Gb\xi}{8\pi\sigma} \right)^{1/2} \quad (5)$$

where  $G$  was the shear modulus. At very large applied stress, the critical span  $l^*$  and the activation volume  $v^*$  leveled off [4]. The strain rate sensitivity  $m$  should thence scale inversely with  $H$ ,

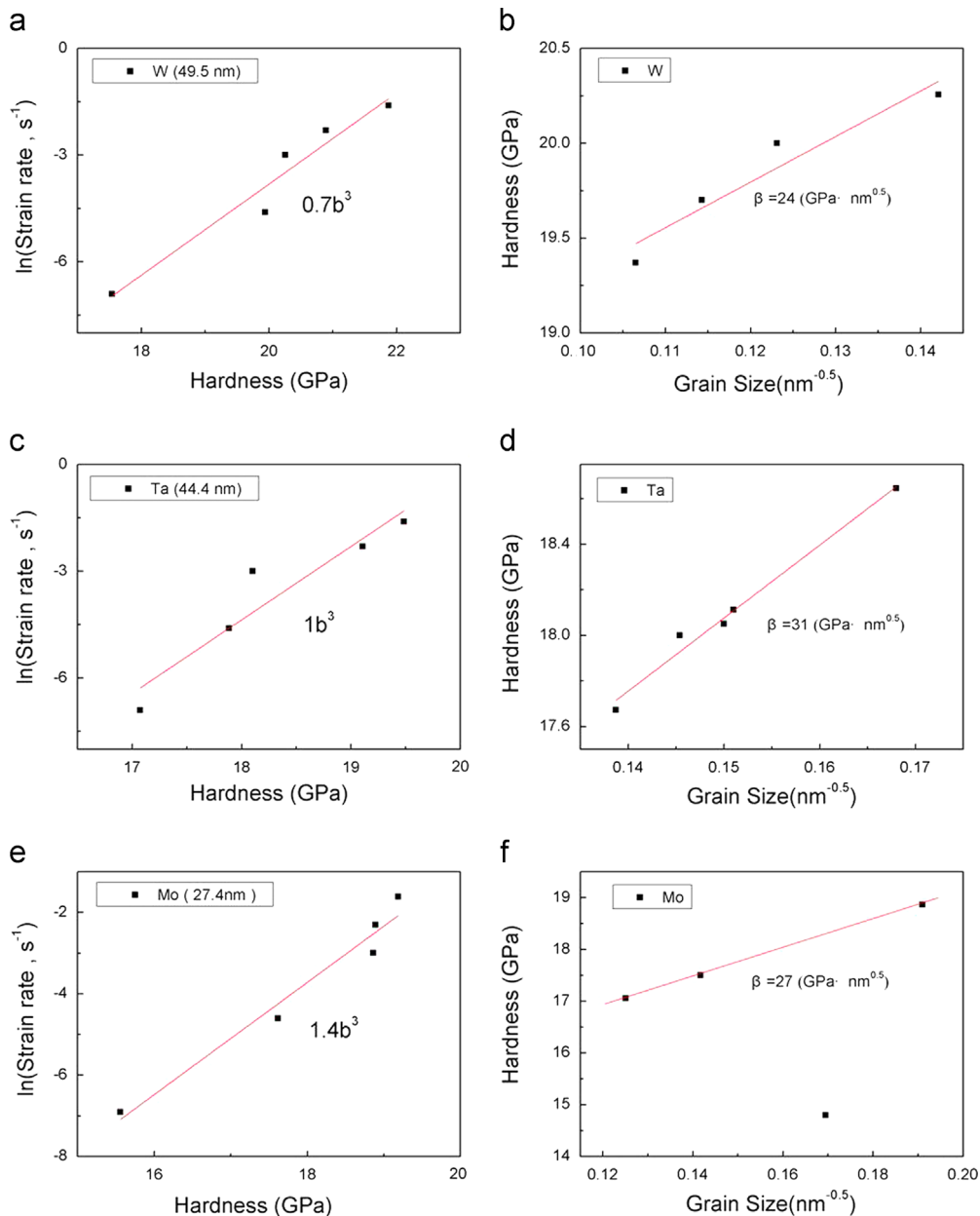


Fig. 6. Experimental results of  $v^*$  and Hall–Petch relationship for nanocrystalline W, Ta and Mo.

following the Hall–Petch relation as

$$H = H_0 + \frac{\beta}{\sqrt{d}} \quad (6)$$

where  $\beta$  was the Hall–Petch coefficient. Substitution of (6) into (4) led to:

$$m = \frac{2.7\sqrt{3}K_b T}{(H_0 + (\beta/\sqrt{d}))v^*} \quad (7)$$

In view of (7), the variation trends observed in Figs. 1b and 5 that  $m$  decreased as the grain size was reduced from coarse-grained to ultra-fine grained regime, were rationalized.

On the other hand, as the grain size was further reduced into the NC regime (below  $d_c$ ), screw dislocation-mediated mechanisms in bcc metals ceased to operate and yielded to GB activities. Here, the critical span depended strongly on grain size  $d$  as [4]:

$$l^* = \chi d \quad (8)$$

where  $l^*$  was likely to be the controlling length scale at very low dislocation densities and  $\chi$  was a proportionality factor [4]. Therefore,  $v^*$  was no longer constant and the variation of  $m$  had to be calculated through  $H \times l^*$ . As the lattice friction  $H_0$  (i.e., intrinsic hardness estimated from coarse-grained bcc metals) was much smaller than  $\beta/\sqrt{d}$  for most bcc metals [29], it was ignored so that:

$$H \times l^* = \left( H_0 + \frac{\beta}{\sqrt{d}} \right) \chi d \approx \beta \chi \sqrt{d} \quad (9)$$

Along with Eqs. (3) and (4), the strain rate sensitivity  $m$  could be approximately expressed as

$$m = \frac{2.7\sqrt{3}K_b T}{b\xi\beta\chi\sqrt{d}} \quad (10)$$

When the grain size decreased into the NC regime, Eq. (10) indicated that  $m$  should increase with decreasing grain size, consistent with the experimentally observed trend as displayed in Fig. 5. To further analyze the dependence of strain rate sensitivity upon grain size, the apparent activation volume in indentation test was calculated as

$$v^* = 2.7\sqrt{3}kT \left( \frac{\partial \ln \dot{\epsilon}}{\partial \ln \dot{H}} \right) \quad (11)$$

where  $k$  was the Boltzmann constant and  $T$  was the absolute temperature. The calculated  $v^*$  of a few examples and Hall–Petch relationship for the three bcc metals were shown in Fig. 6. For NC bcc films, the extremely small apparent activation volume ( $\sim 1b^3$ ) may indeed suggest that the dominant plastic deformation mechanism was the GB-related processes. In addition, the results of Fig. 6 demonstrated that the three bcc metals considered in the present study all obeyed the classical Hall–Petch relationship. The relatively high  $\beta$  in bcc metals may be attributed to the high activation energy required for dislocations nucleation [29]. Further, as an approximation, with  $\chi = b/d_c$  estimated to be 0.03 for W, 0.04 for Ta and 0.05 for Mo and  $K_b = 1.38 \times 10^{-23}$  J/K,  $\xi = b = 2.74$  nm for W, 2.85 nm for Ta, 2.73 nm for Mo,  $\beta = 24$  GPa nm<sup>1/2</sup> for W, 31 GPa nm<sup>1/2</sup> for Ta, 27 GPa nm<sup>1/2</sup> for Mo (Fig. 6 of this work), the  $m$  values calculated from Eq. (9) were compared with those measured in experimentally data, as shown in Fig. 5.

From Fig. 5 it was seen that the predictions from Eq. (10) agreed well with test data at small  $d$ . In this case, as  $d$  dropped into the nanoscale (e.g., less than  $\sim 100$  nm), the screw dislocation density in the grain interior should be very low, whereas the obstacle density associated with GBs increased significantly. It was then difficult for kink-pair nucleation to operate, hence leaving little room for screw dislocation to spread. Under such circumstances, atomic diffusion in the boundary and plastic deformation caused

by stress concentration due to the cut of screw dislocations at the GBs may become the rate controlling processes. At large grain sizes, however, the GB-related model significantly overestimated  $m$  (see in Fig. 5), which may be attributed to the omission of lattice friction in Eq. (8). Nevertheless, more sound explanations about the estimation of strain rate sensitivity are required in the future works.

#### 4. Conclusion

Nanoindentation tests were performed on NC W, Ta and Mo thin metal films. A critical transition grain size, below which the strain rate sensitivity of each NC bcc metal increased with further decreasing grain size, was identified. As the grain size decreased into the  $\sim 50$ – $100$  nm regime, the values of  $m$  and the corresponding  $v^*$  derived for the three bcc metals demonstrated that GB-related mechanisms took over the dislocation-related mechanisms in conventional bcc metals.

#### Acknowledgment

The present work was supported by the National Natural Science Foundation of China (51171141, 51271141), Program for New Century Excellent Talents in University (NCET-11-0431), Research Fund for the Doctoral Program of Higher Education of China (20120201110001).

#### References

- [1] M.A. Meyers, A. Mishra, D.J. Benson, Prog. Mater. Sci. 51 (2006) 427–556.
- [2] M. Dao, L. Lu, R.J. Asaro, J.T.M. De Hosson, E. Ma, Acta Mater. 55 (2007) 4041–4065.
- [3] T. Zhu, J. Li, Prog. Mater. Sci. 55 (2010) 710–757.
- [4] Q. Wei, S. Cheng, K.T. Ramesh, E. Ma, Mater. Sci. Eng. A 381 (2004) 71–79.
- [5] L. Lu, S.X. Li, K. Lu, Scr. Mater. 45 (2001) 1163–1169.
- [6] J. Chen, L. Lu, K. Lu, Scr. Mater. 54 (2006) 1913–1918.
- [7] A.J. Kalkman, A.H. Verbruggen, S. Radelaar, J. Appl. Phys. 92 (2002) 6612–6615.
- [8] H. Miyamoto, K. Ota, T. Mimaki, Scr. Mater. 54 (2006) 1721–1725.
- [9] Y. Wang, A. Hamza, E. Ma, Acta Mater. 54 (2006) 2715–2726.
- [10] F. Dalla Torre, P. Spatig, R. Schaublin, M. Victoria, Acta Mater. 53 (2005) 2337–2349.
- [11] R.J. Asaro, S. Suresh, Acta Mater. 53 (2005) 3369–3382.
- [12] H. Van Swynghevoen, P.M. Derlet, A.G. Frøseth, Acta Mater. 54 (2006) 1975–1983.
- [13] D. Jia, K.T. Ramesh, E. Ma, Acta Mater. 51 (2003) 495–3509.
- [14] Q. Wei, L. Kecskes, T. Jiao, K.T. Hartwig, K.T. Ramesh, E. Ma, Acta Mater. 52 (2004) 1859–1869.
- [15] Q. Wei, T. Jiao, S.N. Mathaudhu, E. Ma, K.T. Hartwig, K.T. Ramesh, Mater. Sci. Eng. A 358 (2003) 266–272.
- [16] Q. Wei, K.T. Ramesh, E. Ma, L.J. Kecskes, R.J. Dowding, Appl. Phys. Lett. 86 (2005) 101907.
- [17] Q. Wei, T. Jiao, K.T. Ramesh, E. Ma, Scr. Mater. 50 (2004) 359–364.
- [18] T.R. Malow, C.C. Koch, P.Q. Miraglia, K.L. Murty, Mater. Sci. Eng. A 252 (1998) 36–43.
- [19] M. Jin, A.M. Minor, E.A. Stach, J.W. Morris Jr, Acta Mater. 52 (2004) 5381–5387.
- [20] B.N. Lucas, W.C. Oliver, Metall. Mater. Trans. A 30A (1999) 601–610.
- [21] Meimei Li, M. Eldrup, T.S. Byun, N. Hashimoto, L.L. Snead, S.J. Zinkle, J. Nucl. Mater. 376 (2008) 11–28.
- [22] T.R. Malow, C.C. Koch, Metall. Mater. Trans. A 29A (1998) 2285–2295.
- [23] T.O. Erinosh, A.C.F. Cocks, F.P.E. Dunne, Int. J. Plasticity 50 (2013) 1–19.
- [24] M.S. Duesbery, W. Xu, Acta Metall. 39 (1998) 283–287.
- [25] J.W. Cahn, F.R.N. Nabarro, Philos. Mag. A 81 (2001) 1409–1426.
- [26] A.H.W. Ngan, M. Wen, Comput. Mater. Sci. 23 (2002) 139–145.
- [27] J.P. Hirth, J. Lothe, Theory of dislocations, Krieger Publishing Company, Malabar, FL, 1992.
- [28] R.J. Arsenault, Acta Metall. 15 (1967) 501–511.
- [29] D. Wu, J.C. Junyan Zhang, H. Huang, Beid, T.G. Nieh, Scr. Mater. 68 (2013) 118–121.
- [30] Q. Wei, Z.L. Pan, X.L. Wu, B.E. Schuster, L.J. Kecskes, R.Z. Valiev, Acta Mater. 59 (2011) 2423–2436.
- [31] A.S. Schneider, B.G. Clark, C.P. Frick, P.A. Gruber, E. Arzt, Mater. Sci. Eng. A508 (2009) 241–246.